LETTER

Dramatic Increase in Fatigue Life in Hierarchical Graphene Composites

F. Yavari, M. A. Rafiee, J. Rafiee, Z.-Z. Yu,* and N. Koratkar*

Department of Mechanical, Aerospace and Nuclear Engineering, Rensselaer Polytechnic Institute, 110 8th Street, Troy, New York 12180-3590, United States, and State Key Laboratory of Chemical Resource Engineering, College of Materials Science and Engineering, Beijing University of Chemical Technology, Beijing 100029, China

ABSTRACT We report the synthesis and fatigue characterization of fiberglass/epoxy composites with various weight fractions of graphene platelets infiltrated into the epoxy resin as well as directly spray-coated on to the glass microfibers. Remarkably only ~0.2% (with respect to the epoxy resin weight and ~0.02% with respect to the entire laminate weight) of graphene additives enhanced the fatigue life of the composite in the flexural bending mode by up to 1200-fold. By contrast, under uniaxial tensile fatigue conditions, the graphene fillers resulted in ~3−5-fold increase in fatigue life. The fatigue life increase (in the flexural bending mode) with graphene additives was ~1−2 orders of magnitude superior to those obtained using carbon nanotubes. In situ ultrasound analysis of the nanocomposite during the cyclic fatigue test suggests that the graphene network toughens the fiberglass/epoxy-matrix interface and prevents the delamination/buckling of the glass microfibers under compressive stress. Such fatigue-resistant hierarchical materials show potential to improve the safety, reliability, and cost effectiveness of fiber-reinforced composites that are increasingly the material of choice in the aerospace, automotive, marine, sports, biomedical, and wind energy industries.

KEYWORDS: graphene • carbon nanotubes • hierarchical nanocomposites • fatigue life

INTRODUCTION

Fiber-reinforced composites (FRC) with their favorable strength-to-weight and stiffness-to-weight ratios are replacing their metal counterparts in a variety of high-performance structural applications (1, 2). However, the principal limitation of FRCs is their brittle failure and insufficient fatigue life, which results in deficiencies in terms of performance, cost, safety, and reliability of structural components (2−4). Consequently, there is great interest in developing new concepts for fatigue-resistant FRC composite materials. One of the emerging industries where such new fatigue resistant materials can have high impact is in wind energy (5). Wind turbine blades are typically composed of glass or carbon-fiber epoxy composites and are prone to fatigue failure because of large cyclic bending loads encountered by the blades during regular operation. Wind is the fastest growing energy technology (~$50 billion investment in 2008) (5) on the globe and enhancing the fatigue properties and the operating life of FRC materials used in wind turbine construction is therefore of great practical relevance.

Matrix modification using micro- or nanostructured fillers (e.g., fumed silica, exfoliated silicate, and carbon nanotubes) (6, 7) has been utilized to enhance the mechanical properties of FRC. Up to ~16% improvement in interlaminar shear strength of FRC composites has been reported (6) by adding ~0.3% weight of carbon nanotubes to the matrix. However, these studies have focused on static properties (strength, modulus, etc.) and fatigue life cycle analysis of such composites has not been performed. Moreover, the use of graphene in FRC systems has not been investigated so far. Here, we report the effect of incorporation of graphene platelets (8−14) on the fatigue life of traditional glass-fiber/epoxy composites. The graphene platelets are introduced into the composite by two methods: (1) by infiltration into the epoxy resin matrix that serves to bind the individual glass-fiber lamina and (2) by directly spraying the graphene platelets on the glass microfibers prior to curing the composite. The hierarchical 3-phase (glass-fiber/epoxy/graphene) composites are fatigue tested in both the uniaxial tension and the flexural bending modes and compared to the conventional 2-phase (glass-fiber/epoxy) composites. We also investigated multiwalled and singlewalled carbon nanotubes as the nanofiller and compared their performance to graphene platelets at the same nanofiller loading (i.e., weight) fraction. In situ ultrasonic C-scan analysis was also performed in order to understand the fatigue suppression mechanism.

RESULTS AND DISCUSSION

Bulk quantities of graphene platelets (GPL) were produced by the thermal reduction (15−18) of graphite oxide. The protocols used to oxidize graphite to graphite oxide and then generate GPL by the thermal exfoliation of graphite oxide are provided in the Experimental Section. Transmission electron microscopy (TEM) of the GPL is shown in Figure 1a; the platelets were observed to be several micrometers in size. Note the wrinkled (rough) surface texture of the GPL which could play an important role in enhancing mechanical interlocking and load transfer with the matrix (9). Raman analysis (Supporting Information) of the GPL indicated an intense D band and significant broadening of both the D and

* Corresponding author. E-mail: yuzz@mail.buct.edu.cn (Z.-Z.Y.); koratn@rpi.edu (N.K.).

Received for review August 13, 2010 and accepted September 17, 2010

DOI: 10.1021/am100728r

Published on Web 09/23/2010

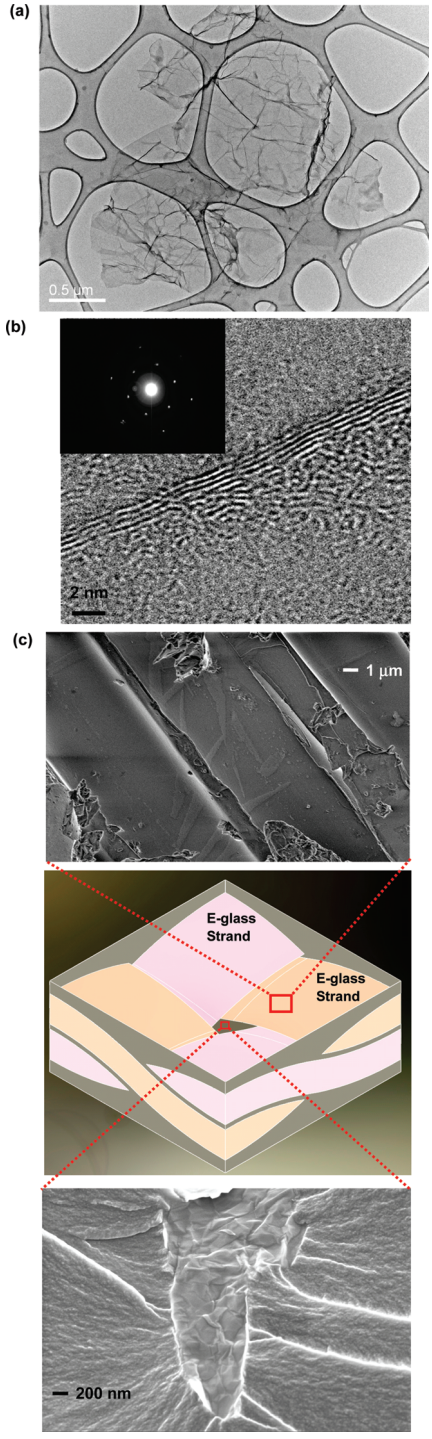

FIGURE 1. Characterization of graphene platelets (GPL) and glass-fiber/epoxy/GPL composites. (a) Transmission electron microscopy (TEM) image of a typical GPL flake deposited on a standard TEM grid for imaging. (b) High-resolution TEM (HRTEM) image of a typical GPL flake showing ~3−4 graphene layers in each platelet. The inset shows the measured electron diffraction pattern which is typical for few-layered graphene. (c) Schematic representation of the unit cell that constitutes the 3-phase hierarchical composite. The three phases include interwoven E-glass strands laid up in the 0−90 direction, epoxy matrix that serves as the binder and GPL dispersed into the epoxy matrix. Top Scanning electron microscopy (SEM) image shows individual microscale glass fibers within the woven fabric strand. GPL additives interlinking the glass fibers through the epoxy matrix are also discernable. Lower SEM image shows a typical GPL/epoxy-matrix interface obtained from the matrix-rich region of the composite; there is no indication of interfacial debonding, which suggests a strong interface.

G bands indicating a high degree of disorder (19). This appears to be an artifact of the oxidation of graphite and the thermal shock that was employed to exfoliate graphite oxide to graphene. Figure 1b shows a typical high-resolution TEM (HRTEM) image of the GPL edge structure indicating that each platelet is composed of ~3−4 individual graphene sheets. The electron diffraction pattern (inset of Figure 1b) confirms the signature of few-layered graphene. Nitrogen cryosorption experiments were also performed on the GPL powder and the corresponding specific surface area was calculated using Brunauer-Emmett-Teller (BET) theory as ~720 m^2/g (Supplementary Information). This is ~3.5 times smaller than the specific surface area (~2630 m^2/g) of an idealized (single) graphene sheet (15, 16), which confirms the HRTEM observation that the graphene platelets are composed on average of ~3−4 graphene layers.

The hierarchical composites synthesized in this study consist of E-glass woven fabric plies (bidirectional, twill weave, style 7725 from Fibreglast, USA) paired with a Bisphenol-A based epoxy matrix (Epoxy 2000 from Fibreglast, USA) that is infused with a graphene network. The first step in the fabrication of these composites is to disperse the as-produced GPL in the thermosetting epoxy resin via ultrasonication (Experimental Section). Then the GPL/epoxy blend is painted layer-by-layer on the glass-fibers; eight fiberglass plies were used to construct the composite laminate. After all of the woven fabric glass-fiber plies were laid up (0−90 direction) and wetted with the GPL infused epoxy, a vacuum bag was placed over the system, and the sample was cured under vacuum for 24 h at room temperature. During this process, excess epoxy is extracted out of the composite into an absorbent cloth. Lastly, the composite is taken out of the vacuum bag and placed in an oven at 90°C for high temperature cure for four hours. The estimated volume fraction of the glass micro-fibers in the composite structure was ~0.8. The weight fraction of epoxy in the composite is estimated as ~10%. Figure 1c illustrates a schematic of the unit cell along with scanning electron microscopy (SEM) images indicating the three main phases of the composite: i.e., the E-glass fibers, the epoxy matrix and the GPL in the matrix-rich regions (bottom SEM) as well as GPL interlinking the individual glass fibers within a strand (top SEM). There is no indication of GPL pull-out from the epoxy matrix, suggesting a strong interface. This is supported by loss modulus vs temperature measurements (not shown here) which indicated ~10° C rise in the glass transition temperature of the neat epoxy resin with only ~0.1% weight of GPL.

The hierarchical glass-fiber/epoxy/GPL laminates were fatigue tested in a 3-point bend test configuration as shown schematically in the inset of Figure 2a. The cyclic loading tests were performed at a frequency of ~5 Hz and the stress ratio (R: minimum-to-maximum applied stress) was 0.1. We plot the maximum bending stress (S) vs the number of cycles to failure (N) for the hierarchical composite for various GPL weight fractions up to a maximum of 0.2%. Note that 0.2% is the weight fraction of GPL in the epoxy resin. The weight

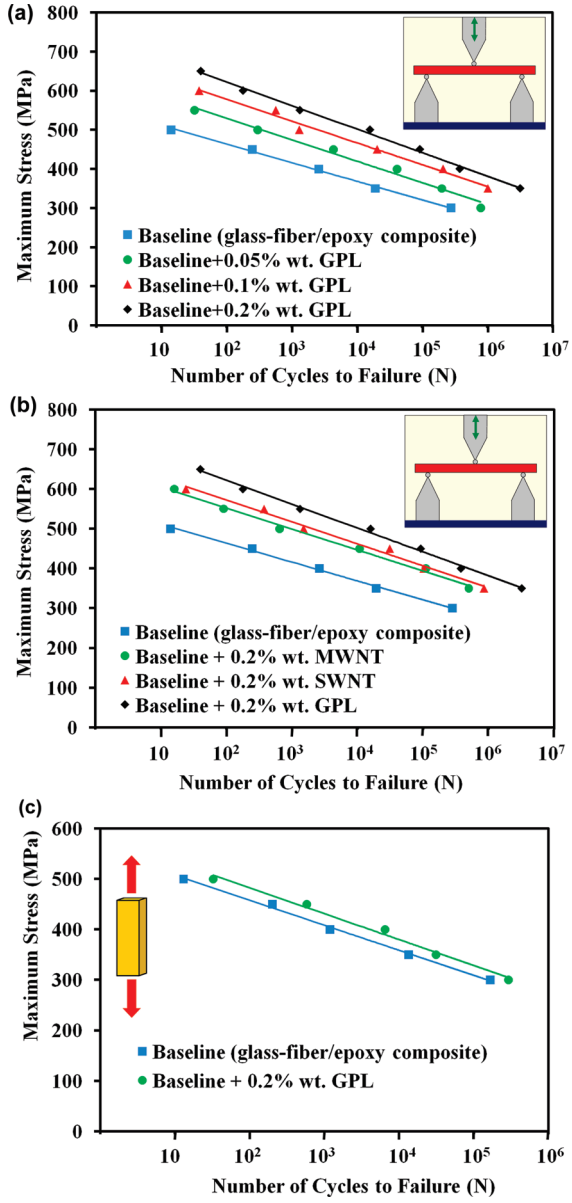

FIGURE 2. Fatigue characterization results. (a) Maximum bending stress (S) vs number of cycles to failure (N) for baseline glass-fiber/epoxy composites and glass-fiber/epoxy/GPL composites with various weight fractions of GPL in the epoxy resin. The test is performed in the flexural bending mode as indicated in the inset schematic. (b) $S-N$ curve comparing the fatigue response in flexural bending mode of GPL with SWNT and MWNT additives at the same weight fraction of ~0.2% of the epoxy resin weight. (c) $S-N$ fatigue curve in pure tension mode (i.e., no compressive stress) for baseline glass-fiber/epoxy and glass-fiber/epoxy/GPL composites. GPL weight fraction is ~0.2% of the epoxy resin weight.

fraction of GPL in the entire laminate (including the E-glass microfibers) was estimated to be an order of magnitude lower (~0.02% for ~0.2% weight of GPL in the epoxy). At each stress level, a minimum of three samples with the same GPL loading were tested to failure and the averaged results are represented as $S-N$ curves (Figure 2a). The results indicate a significant increase in the number of cycles to failure across the entire range of applied stresses. Increasing the GPL weight fraction from 0.05 to 0.2% had a strong beneficial impact on the fatigue life enhancement. At a stress level of ~500 MPa, the fatigue life of the composite with ~0.2% by weight of GPL in the epoxy resin is enhanced by ~1200-fold as compared to the baseline glass-fiber/epoxy composite without the GPL. At lower stress levels (<400 MPa) we measured about two orders of magnitude increase in fatigue life of the hierarchical composite relative to the baseline. Figure 2b compares the performance of GPL with singlewalled carbon nanotube (SWNT) and multiwalled carbon nanotube (MWNT) reinforcement at a constant nanofiller weight fraction of ~0.2%. The processing conditions used for SWNT and MWNT composites were identical to that of graphene. Depending on the applied stress, GPL offers 1−2 orders of magnitude increase in fatigue life as compared to MWNT and SWNT at the same weight fraction of additives. We also performed fatigue tests on hierarchical composites in the uniaxial tensile mode (no compressive loading). For these cases (Figure 2c) we do observe an enhancement in fatigue life, but the improvements were relatively modest (~3−5 times increase depending on the stress level) compared to the flexural bending fatigue results shown in panels a and b in Figure 2.

We also measured static properties (such as flexural modulus and flexural strength) of the hierarchical and baseline composites. There was a ~20−30% increase in flexural strength (see the Supporting Information), whereas the flexural modulus remained unchanged for the hierarchical and baseline composites. The static tensile modulus and tensile strength of the hierarchical and baseline composites also showed no significant differences. Many studies (4, 11, 20, 21) have shown that there is a huge difference between static and dynamic results especially with respect to fatigue. For example, in ref 11, epoxy/graphene composites with ~0.1% weight of multilayer graphene platelets enhanced the fracture toughness of the baseline epoxy by ~53%, whereas the dynamic fatigue crack propagation rate was suppressed by up to two orders of magnitude (~100-fold). In our hierarchical system, if the graphene platelets are suppressing the propagation rate of inter-laminar fatigue cracks by ~100-fold, it is then conceivable that the total lifetime of the component (which involves the dynamic growth of such fatigue cracks and delaminations to critical dimensions) can also be enhanced by 2−3 orders of magnitude.

To better understand the mechanism(s) responsible for the three orders of magnitude increase in fatigue life that we observe, we performed ultrasonic C-scans (22, 23) of the samples prior to beginning the test as well as during the fatigue test. Figure 3a illustrates a typical ultrasound image of the longitudinal cross-section of the sample prior to fatigue loading. The image indicates a high degree of uniformity in the sample with absence of significant defects (voids) in the material. Figure 3b shows an ultrasound scan after 200 000 cycles of fatigue loading for the baseline glass-fiber/epoxy composite (no GPL) at a maximum bending stress of ~300 MPa. The image shows a stark contrast between the tension side and the compression side of the sample. On the tension side there is relatively less accumulation of damage to the sample, while on the compression side a large increase in porosity is observed suggesting delamination of the glass-

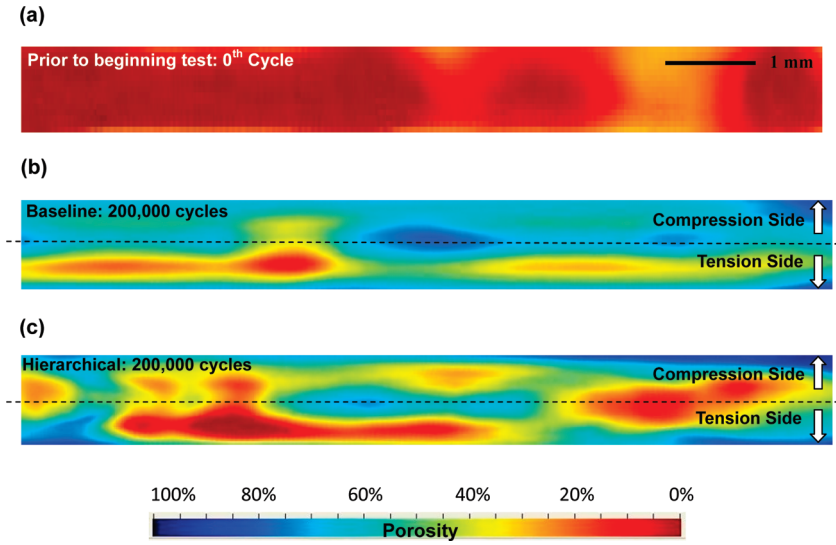

FIGURE 3. Mechanism for fatigue enhancement. (a) Ultrasound analysis of the longitudinal cross-section of a typical sample prior to fatigue loading. Red indicates 0% porosity, whereas blue indicates 100% porosity in the sample. (b) Ultrasound analysis of baseline glass-fiber/epoxy sample after 200 000 cycles of fatigue loading in bending mode at ~300 MPa peak bending stress. The tension (bottom) and compression (top) sides as well as the neutral axis of the sample cross-section are marked out for clarity. (c) Corresponding ultrasound results for glass-fiber/epoxy/GPL sample with ~0.2% weight of GPL after 200 000 cycles of fatigue loading in bending mode at ~300 MPa peak bending stress. Scale bar indicated in panel a also applies to panels b and c.

fiber/epoxy-matrix interface. Such debonding is typically caused by interlaminar crack propagation (24−26) and the buckling of the glass-fibers (27, 28) under compressive load. This results in large voids (i.e., damage) in the material as seen in the ultrasound images. The extent of damage on the compression side for the hierarchical glass-fiber/epoxy/GPL composite (also loaded for 200 000 cycles at ~300 MPa peak bending stress) is markedly lower than the baseline composite as indicated in the ultrasound scan of Figure 3c. The average porosity on the compression side after 200 000 cycles of fatigue loading for the hierarchical graphene composite is ~42 % (Figure 3c) compared to ~71 % (Figure 3b) for the baseline composite. Moreover, in contrast to the baseline, there is no longer a large difference in "damage accumulation" between the tension side and the compression side of the sample during the flexural bending fatigue test. These results suggest that the main mechanism for prolonged fatigue life for the hierarchical composite appears to lie in the ability of the GPL to suppress interlaminar crack propagation and delamination/buckling of the fiberglass/epoxy matrix interface under compressive stress. A similar phenomena is also expected in the case of carbon nanotubes, however this effect is far stronger for GPL (figure 2b), likely due to several reasons: (1) GPL has a rough and wrinkled surface topology (see Figure 1a), which can enable it to mechanically interlock (9) with the glass-fibers and the epoxy matrix far more effectively than the atomistically smooth carbon nanotubes. Moreover GPL produced by thermal reduction of graphite oxide (8, 9) has residual hydroxyl and epoxide functional groups, which could interact covalently with the epoxy chains, thereby further promoting interfacial adhesion. (2) The specific surface area of GPL powder (>700 m^2/g) is larger compared to nanotubes (in bulk powder form SWNT and MWNT show specific area in the range of 229−429 m^2/g) (29). (3) The micrometer size dimensions, high aspect ratio, and two-dimensional sheet geometry of GPL makes it highly effective at deflecting cracks and GPL has been shown to be superior (11, 12) to SWNT and MWNT in terms of toughening the epoxy matrix.

Under pure tensile fatigue, the microfiber/matrix interface is less important because unlike in compression, the microfibers are more effective (30) than the matrix in carrying tensile loads. Consequently, maintaining the integrity of the microfiber/matrix interface while critical to boosting the fatigue life of the composite in bending/shear or direct compression is relatively less important under pure tension (as observed in Figure 2c). This analysis also suggests that the optimal placement of the GPL additives is right at the microfiber/matrix interface for maximum effectiveness. To test this hypothesis, we explored an alternative method for fabrication of the hierarchical composites. In this method, we dispersed the GPL in acetone via sonication (Materials & Methods) and then directly sprayed the GPL platelets on to the glass-fibers. The regular epoxy (without any GPL additives) was then applied layer-by-layer to the GPL-coated glass-fibers and then cured. This method has two advantages: (1) there is a greater concentration of graphene sheets near the glass-fiber/epoxy interface and (2) the epoxy without the nanofillers is less viscous and therefore easier to work with. As expected locating the GPL fillers closer to the glass-fiber/matrix interface results in significant enhancement in fatigue life (see Figure 4) over uniformly dispersing them in the bulk epoxy resin. For the case of 0.2 % of GPL (measured with respect to the epoxy resin weight required to cure the composite) but directly spray-coated on to the glass microfibers, we observe that the number of cycles to failure at a bending stress of ~400 MPa is ~3 000 000 which is ~8-times greater than when the GPL are uniformly dispersed in the resin and ~1250-times greater than the fatigue life of

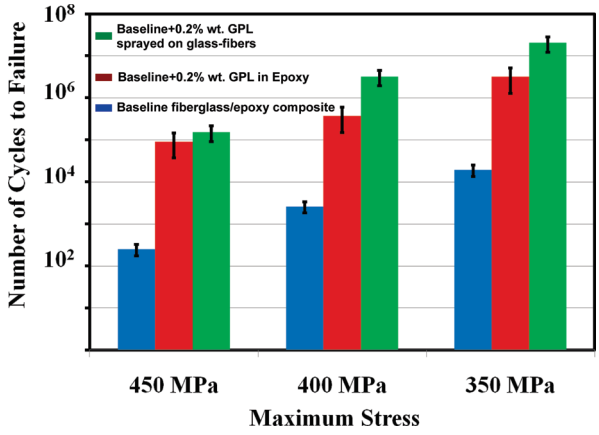

FIGURE 4. Flexural bending fatigue results comparing performance of three-phase composites with GPL dispersed into the bulk resin vs. the same amount of GPL by weight directly spray-coated onto the glass microfibers. Data is shown at various peak bending stress levels. Directly spray-coating the GPL at the fiber-matrix interface yields significant benefit over uniform dispersion of GPL in the bulk epoxy resin.

the baseline glass-fiber/epoxy composite without any GPL reinforcement.

CONCLUSIONS

The over three orders of magnitude enhancement in the flexural bending fatigue life of conventional microfiber reinforced polymer composites achieved by the use of graphene platelets can translate into significant performance, cost, safety and reliability benefits in a wide range of structural applications. The relatively low weight fractions of graphene additives (~0.2 % of the epoxy resin weight and ~0.02 % of the entire laminate weight) that are required as well as the ability to directly spray-coat the graphene fillers on to the microfiber lamina could make this concept particularly suitable for large-scale industrial applications in the aerospace, automobile, marine, and wind energy industries.

EXPERIMENTAL SECTION

Natural graphite flakes with an average diameter of 48 μm were supplied from Huadong Graphite Factory (Pingdu, China). Concentrated sulfuric acid (95−98 %), concentrated nitric acid (68 %) and hydrochloric acid (36−38 %) were purchased from Beijing Chemical Factory, China. Potassium chlorate (99.5 %) was obtained from Fuchen Chemical Reagents (Tianjin, China). The epoxy used in the present study was a Bisphenol-A based epoxy (Epoxy 2000 from Fibreglast, USA) and the curing agent used was 2120 Epoxy Hardener from Fibreglast, USA. The singlewalled carbon nanotubes (SWNT, purity >95 %) used in this study were provided by Cheap Tube Inc. with a mean diameter of ~2 nm and length of ~10 μm. Multiwalled carbon nanotubes (MWNT, purity >95 %) were provided by Nanocyl with a mean diameter of ~20 nm and length of ~20 μm. The fiberglass used was a fabric (bidirectional E-glass, twill weave, style 7725) obtained from Fibreglast, USA.

Graphite oxide was prepared by oxidizing graphite in a solution of sulfuric acid, nitric acid and potassium chlorate for 96 h (15−17). X-ray diffraction patterns of natural graphite and graphite oxide are provided in the Supporting Information. Thermal exfoliation of graphite oxide was achieved by placing the graphite oxide powder (200 mg) in a 200 mm inner diameter, 1 m long quartz tube that was sealed at one end. The other end of the quartz tube was closed using a rubber stopper. An argon inlet was then inserted through the rubber stopper. The sample was flushed with argon for 10 min, and the quartz tube was quickly inserted into a tube furnace (Thermolyne 79300, Thermo Fisher Scientific Inc., USA) preheated to 1050 °C and held in the furnace for ~35 s. Raman spectroscopy and BET surface area analysis of the GPL are provided in the Supporting Information file.

GPL was dispersed in acetone (100 mL of acetone to 0.1 grams of GPL) using an ultrasonic probe sonicator at high amplitude (Sonics Vibracell VC 750, Sonics and Materials Inc., USA) for 1.5 h in an ice bath. The epoxy (System 2000 Epoxy Resin, Fibreglast Inc, USA) was added to the mixture, and sonicated following the same procedure for another 1.5 h. Next, the acetone is evaporated off by heating the mixture on a magnetic stir plate using a Teflon coated magnetic bar for 3 h at 70°C. The mixture is placed in a vacuum chamber for 12 h at 70°C to ensure that all of the acetone has been removed. After allowing the GPL/epoxy slurry to cool down to room temperature to prevent any premature curing, a low viscosity curing agent (2120 Epoxy Hardener, Fibreglast Inc, USA) is added and mixed using a high speed shear mixer (ARE-250, Thinky, Japan) for two minutes at 2000 rpm. The mixture is again placed in a vacuum chamber to degas the epoxy for approximately 30 min. This epoxy/GPL blend is then applied layer-by-layer to wet the individual E-glass fiber lamina and then the composite laminate is cured at room temperature for 24 h using standard vacuum bagging techniques followed by four hours of post-cure at 90° C. For both the flexural bending and the tensile fatigue tests, the stress ratio (R, ratio of the minimum applied stress to maximum applied stress) was equal to 0.1. The fatigue tests were performed at a frequency of ~5 Hz using our MTS-858 servo-hydraulic test facility.

Acknowledgment. N.K. acknowledges funding support from the U.S. Office of Naval Research (Award Number: N000140910928) and the U.S. National Science Foundation (Award 0900188).

Supporting Information Available: X-ray diffraction of graphite and graphite oxide, Raman spectra of graphene platelets, nitrogen cryo-sorption data on bulk graphene powder, scanning electron micrograph of the fatigue-fractured sample, and static flexural strength measurements for the baseline and hierarchical nanocomposites (PDF). This material is available free of charge via the Internet at http://pubs.acs.org.

REFERENCES AND NOTES

(1) Garg, A. C.; Mai, Y.-W. *Compos. Sci. Technol.* **1988**, *31*, 179–223.
(2) Argon, A. S.; Cohen, R. E. *Polymer* **2003**, *44*, 6013–6032.
(3) Pearson, R. A.; Yee, A. F. *J. Mater. Sci.* **1989**, *24*, 2571–2580.
(4) Zhang, W.; Srivastava, I.; Zhu, Y.-F.; Picu, C. R.; Koratkar, N. *Small* **2009**, *5*, 1403–1407.
(5) Kong, C.; Bang, J.; Sugiyama, Y. *Energy.* **2005**, *30*, 2101–2114.

(6) Wichmann, M. H. G.; Sumfleth, J.; Gojny, F. H.; Quaresimin, M.; Fiedler, B.; Schulte, K. *Eng. Fract. Mech.* **2006**, *73*, 2346–2359.
(7) Vlasveld, D. P. N.; Parlevliet, P. P.; Bersee, H. E. N.; Picken, S. J. *Composites Part A* **2005**, *36*, 1–11.
(8) Stankovich, S.; Dikin, D. A.; Dommett, G. H. B.; Kohlhaas, K. M.; Zimney, E. J.; Stach, E. A.; Piner, R. D.; Nguyen, S. T.; Ruoff, R. S. *Nature* **2006**, *442*, 282–286.
(9) Ramanathan, T.; Abdala, A. A.; Stankovich, S.; Dikin, D. A.; Herrera-Alonso, M.; Piner, R. D.; Adamson, D. H.; Schniepp, H. C.; Chen, X.; Ruoff, R. S.; Nguyen, S. T.; Aksay, I. A.; Prud'Homme, R. K.; Brinson, L. C. *Nat. Nanotechnol.* **2008**, *3*, 327–331.
(10) Williams, G.; Seger, B.; Kamat, P. V. *ACS Nano* **2008**, *2*, 1487–1491.
(11) Rafiee, M. A.; Rafiee, J.; Wang, Z.; Song, H.; Yu, Z.-Z.; Koratkar, N. *ACS Nano* **2009**, *3*, 3884–3890.
(12) Rafiee, M. A.; Rafiee, J.; Srivastava, I.; Wang, Z.; Song, H.; Yu, Z.-Z.; Koratkar, N. *Small* **2010**, *6*, 179–183.
(13) Wang, D.-W.; Li, F.; Zhao, J.; Ren, W.; Chen, Z.-G.; Tan, J.; Wu, Z.-S.; Gentle, I.; Lu, G. Q.; Cheng, H.-M. *ACS Nano* **2009**, *3*, 1745–1752.
(14) Gong, L.; Kinloch, I. A.; Young, R. J.; Riaz, I.; Jalil, R.; Novoselov, K. S. *Adv. Mater.* **2010**, *22*, 2694–2697.
(15) Schniepp, H. C.; Li, J.-L.; McAllister, M. J.; Sai, H.; Herrera-Alonso, M.; Adamson, D. H.; Prud'homme, R. K.; Car, R.; Saville, D. A.; Aksay, I. A. *J. Phys. Chem. B* **2006**, *110*, 8535–8539.
(16) McAllister, M. J.; Li, J.-L.; Adamson, D. H.; Schniepp, H. C.; Abdala, A. A.; Liu, J.; Herrera-Alonso, M.; Milius, D. L.; Car, R.; Prud'homme, R. K.; Aksay, I. A. *Chem. Mater.* **2007**, *19*, 4396–4404.
(17) Rafiee, M.; Rafiee, J.; Yu, Z.-Z.; Koratkar, N. *Adv. Mater.* **2010**, *22*, 2151–2154.
(18) Park, S.; Ruoff, R. S. *Nat. Nanotechnol.* **2009**, *4*, 217–224.
(19) Gupta, A.; Chen, G.; Joshi, P.; Tadigadapa, S.; Eklund, P. C. *Nano Lett.* **2006**, *6*, 2667–2673.
(20) Wetzel, B.; Rosso, P.; Haupert, F.; Friedrich, K. *Eng. Fract. Mech.* **2006**, *73*, 2375–2398.
(21) Blackman, B.; Kinloch, A. J.; Sohn Lee, J.; Taylor, A. C.; Agarwal, R.; Schueneman, G.; Sprenger, S. *J. Mater. Sci.* **2007**, *42*, 7049–7051.
(22) Aymerich, F.; Meili, S. *Composites, Part B* **2000**, *31*, 1–6.
(23) Kas, Y. O.; Kaynak, C. *Polym. Test.* **2005**, *24*, 114–120.
(24) Talreja, R., Ed. *Damage Mechanics of Composite Materials*; Composite Materials Series; Elsevier: Amseterdam, 1994, New York; Vol. 9, pp 139—241.
(25) Kinloch, A. J.; Wang, Y.; Williams, J. G.; Yayla, P. *Compos. Sci. Technol.* **1993**, *47*, 225–237.
(26) Albertsen, H.; Ivens, J.; Peters, P.; Wevers, M.; Verpoest, I. *Compos. Sci. Technol.* **1995**, *54*, 133–145.
(27) Ma, C.; Ji, L. J.; Zhang, R. P.; Zhu, Y. F.; Zhang, W.; Koratkar, N. *Carbon* **2008**, *46*, 706–710.
(28) Tadjbakhsh, I. G.; Wang, Y. M. *Int. J. Solids Struct.* **1992**, *29*, 3169–3183.
(29) Liu, C.; Chen, Y.; Wu, C.-Z.; Xu, S.-T.; Cheng, H.-M. *Carbon* **2010**, *48*, 452–455.
(30) Tanaka, K.; Tanaka, H. *Composite Materials: Fatigue and Fracture, ASTM STP 1285*; Armanios, E. A., Ed.; American Society for Testing and Materials: West Conshohocken, PA, 1997; Vol. 12, pp 6—142.

AM100728R